

Article

The Role of High Water Temperature in the Context of Low-Flow Risk Analysis

Udo Satzinger *  and Daniel Bachmann

Department of Water, Environment, Construction and Safety, Magdeburg-Stendal University of Applied Sciences, 39114 Magdeburg, Germany; daniel.bachmann@h2.de

* Correspondence: udo.satzinger@h2.de; Tel.: +49-391-8864607

Abstract: Low-flow events significantly impact water users and ecosystems due to reduced flow rates and deteriorating water quality. Elevated water temperatures during these periods have led to economic and ecological consequences. Therefore, water temperature is a key aspect in the context of low-flow risk analysis, and it is essential to model it accurately. This study introduces a one-dimensional water temperature model optimized for integration into low-flow risk analysis frameworks. Results demonstrate good performance in simulating water temperatures for both rivers, with Nash–Sutcliffe efficiency values of 0.85–0.98 and root mean square errors of 0.96–1.96 K. The model was evaluated on two contrasting river systems: the small Selke River and the large Elbe River. The model effectively captures anthropogenic influences and altered environmental conditions. Key factors influencing water temperature varied by river size, with tributaries and shading having more impact on smaller rivers, while air temperature was the primary driver for larger rivers. The model’s computational efficiency enables the practical implementation of long-term risk assessments. This temperature model fulfills the requirements for integration into low-flow risk management frameworks, providing a valuable tool for assessing temperature-related impacts and evaluating mitigation strategies across diverse river systems.

Keywords: water temperature; low flow; low-flow risk; consequences; low-flow risk management; temperature modelling; high water temperature; thermal pollution



Academic Editors: Xuan Ban, Wenxian Guo and Yicheng Fu

Received: 10 March 2025

Revised: 15 April 2025

Accepted: 21 April 2025

Published: 22 April 2025

Citation: Satzinger, U.; Bachmann, D. The Role of High Water Temperature in the Context of Low-Flow Risk Analysis. *Water* **2025**, *17*, 1247. <https://doi.org/10.3390/w17091247>

Copyright: © 2025 by the authors. Licensee MDPI, Basel, Switzerland. This article is an open access article distributed under the terms and conditions of the Creative Commons Attribution (CC BY) license (<https://creativecommons.org/licenses/by/4.0/>).

1. Introduction

The low-flow events observed in recent years have resulted in significant consequences for water users and ecosystems. However, in the majority of events, the consequences are not attributable to the complete desiccation of water bodies, but rather to a combination of reduced flow rates and deteriorating water quality. While water availability is often the primary concern during periods of low flow, the water quality is of equal, if not greater, importance. Water temperature is a crucial component of overall water quality. It affects many physical, chemical, and biological processes in aquatic ecosystems. Elevated water temperatures, particularly during periods of low flow, result in significant economic and ecological consequences. In 2018, due to elevated water temperatures exceeding 25 °C in the Rhine, the Fessenheim and Phillipsburg nuclear power plants were compelled to reduce electricity production, as the discharge of cooling water would have resulted in additional thermal pollution to the river [1]. Furthermore, the Chooz and Golfech nuclear power plants in France were compelled to reduce their output and, in some instances, cease operations entirely in 2019, 2020 and 2022 due to elevated water temperatures in the rivers [2–4]. Other extractors were similarly constrained by restrictions; for instance,

irrigation was prohibited in certain regions of Europe to mitigate further increases in water temperatures, resulting in crop losses [5]. The ecological consequences are particularly evident and can be observed through various phenomena. A notable illustration of the interaction between low discharges and poor water quality is the fish die-off in the Oder River in 2022, which was precipitated by the excessive proliferation of a specific algal species. The prevailing low-flow conditions resulted in reduced flow velocities and consequently increased retention times, coupled with diminished dilution capacity, thereby leading to elevated nutrient concentrations. The heightened water temperatures facilitated enhanced metabolic rates, particularly for *Prymnesium parvum*, thus supporting a mass algal boom [6]. Furthermore, there have been increasing ecological consequences observed in other European watercourses. Accordingly, due to enhanced algal proliferation and elevated water temperatures, a significant fish mortality event occurred in an oxbow lake of the river Danube [7]. Similarly, fish mortality events attributed to water temperatures exceeding 27 °C were observed in the upper part of the Rhine in 2018 [1]. However, it was not solely fish that were affected; in smaller rivers, the prolonged low-flow periods and elevated temperatures resulted in increased mortality of aquatic organisms, such as mussels [8].

It is anticipated that the ongoing phenomenon of climate change will exacerbate existing challenges and heighten the demand for effective management strategies [9]. The mentioned consequences demonstrate that the interaction between elevated water temperatures and low flow can exert significant effects. These impacts necessitate mitigation through appropriate measures, which in the case of elevated water temperatures could include shading or the reduction of thermal pollution (e.g., cooling water). To accurately replicate the current state and future alterations and, similarly, when selecting measures, it is necessary to consider all aspects of a low-flow event, which can be accomplished by implementing a holistic low-flow risk analysis. Satzinger and Bachmann (2024) [10] propagate a holistic framework wherein water temperature serves as a critical determinant in assessing low-flow risk. The primary objective is to utilize long-term series rather than scenarios to circumvent the complex definition of the latter. The first step is the meteorological analysis, where synthetic long-term weather data series are produced, which are subsequently transformed into runoff time series within the hydrological analysis. These serve as input data for the hydrodynamic analysis, where flow velocity, water level, and water temperature are calculated. In the analysis of consequences, the economic and ecological impacts are quantified using the results from the hydrodynamic analysis. Ultimately, the damage sum is combined with the probability of occurrence to determine risk within the risk analysis. In this approach, the temperature model plays a crucial role in the hydrodynamic analysis, the analysis of consequences, and, consequently, the risk analysis. Due to the long-term nature of the risk approach on one hand and the temporally detailed temperature data requirements on the other, a model that satisfies both criteria is necessary. This study presents a temperature model that is intended for integration into low-flow risk analysis. Therefore, this study aims to address the following research questions: (i) what role does water temperature play in the context of low-flow conditions, (ii) how can water temperature be effectively determined within a low-flow risk analysis, and (iii) is the implemented model capable of mapping altered circumstances and anthropogenic discharges during low-flow events?

This study adopts the approach of Satzinger and Bachmann (2024) [10] and investigates the role of water temperature in low-flow risk analysis. Initially, a concise overview of the possible consequences of elevated water temperatures in combination with low flow is presented, supplementing those previously mentioned. Subsequently various methodologies for determining the water temperature in aquatic systems are presented,

and the selected model is evaluated along the rivers Selke and Elbe. The resulting findings are categorized and examined within the context of low-flow risk.

To appropriately consider water temperature in the context of low-flow risk management, it is first necessary to determine its role. The focus lies on the nature and extent of the impacts that arise from high water temperatures in interaction with low-flow conditions. van Vliet et al. (2011) [11] show that decreasing discharges during low flow can lead to increased warming of the river. In general, the sensitivity to warming is increased during low flow, which is due to the reduced thermal capacity. These findings are also replicated by other studies. Booker and Whitehead (2022) [12], in an investigation of 47 sampling sites along rivers, demonstrated that water temperatures during low-flow events were significantly higher. Low flow can therefore favor high water temperatures, which in turn cause a range of ecological and economic consequences. A further critical aspect is the occurrence of low-flow periods, which often coincide with episodes of elevated air temperatures and increased solar radiation. This temporal alignment subsequently contributes to additional warming of the river. This phenomenon could be further exacerbated by climate change [13].

From an economic perspective, high water temperatures are problematic in several ways. Rothstein et al. (2008) [14] investigated the effects of low flow and high water temperatures on thermal power plants in Germany. For instance, adherence to the pertinent legal requirements for extraction and discharge is imperative, and this frequently incorporates minimum ecological standards and considerations for alternative water utilization. Another issue associated with elevated river water temperatures is the reduced efficiency of thermal power plants due to the higher ambient temperatures [15]. Furthermore, the elevation of cooling water temperature is anticipated to enhance biofilm formation, consequently leading to increased maintenance requirements and corrosion. As early as the beginning of the 2000s, several thermal power plants in Germany experienced operational restrictions, particularly during the 2003 low-flow event.

The effects of elevated water temperatures on fish and other aquatic organisms have been extensively researched. However, the interaction between low-flow conditions and high water temperatures has been investigated in only a limited number of studies. In their study of North American waters, Arismendi et al. (2013) [16] found that the periods of maximum water temperature and minimum discharge are increasingly converging. This convergence could be further exacerbated by the ongoing changes in the climate. The combination of low water levels and elevated water temperatures results in particularly acute stress for aquatic organisms, as habitats are restricted and reduced in size by the low water levels, and the high temperatures can lead to physiological stress and additional pressure. Elevated temperatures induce alterations in the metabolism of the animals and contribute to a decrease in dissolved oxygen concentration in the river. Bradford and Heinonen (2008) [17] describe various effects of low flow on the ecology of small rivers. Elevated water temperatures can create favorable conditions for invasive species, potentially intensifying competition with native species. Reduced water levels and elevated water temperatures can impede reproduction, as the warming of spawning and juvenile fish habitats may result in increased mortality rates. Organic pollution, in conjunction with elevated water temperatures, can potentially result in excessive plant growth, which may subsequently have detrimental effects on fish and invertebrate populations.

The aforementioned consequences clearly show the eminent influence that high water temperatures can have during low-flow periods. In addition, the effect is further intensified by low water volumes and additional warming takes place. It can be stated that water temperature plays a central role as a parameter within the low-flow risk analysis, especially

as a basis for analyzing the consequences. It is therefore essential to determine water temperatures as realistically as possible.

Various methodologies exist for predicting water temperature in flowing water systems. In addition to statistical models and artificial intelligence, both of which are predicated on measured values and their subsequent analysis, modelling utilizing deterministic or process-based models is also feasible. A selection of exemplars is presented below to provide a concise overview of the diverse approaches available.

Firstly, data-driven models, which are among the most straightforward models to utilize, will be presented. Rabi et al. (2015) [18] describe the utilization of linear regression to calculate water temperature based on air temperature. The stochastic modelling in the study involved predicting river water temperatures as a function of time, separating the temperature data into long-term periodic (seasonal) and short-term components. The results demonstrate an improved predictive ability when employing the stochastic calculation. van Vliet et al. (2011) [11] utilize a non-linear regression and incorporate the discharge as a second parameter in addition to the air temperature in order to accurately capture the influence of the flow on the temperature. The implementation of the two-parameter non-linear regression function demonstrated improved results. A frequently utilized model is the air2stream model developed by Toffolon and Piccolroaz (2015) [19], which employs a hybrid approach. It incorporates the principles of heat transfer and the influence of environmental factors, such as air temperature and discharge, which are crucial for comprehending how these variables affect river water temperature. The model utilizes statistical techniques to adjust the model based on observed data, enabling it to better align with real-world conditions without relying on a large set of empirical relationships. Benyahya et al. (2007) [20] conducted a review of existing statistical approaches for water temperature models.

Zhu et al. (2018) [21] employed three distinct machine learning models to estimate daily water temperatures in the Missouri River. They conducted a comparative analysis with statistical and stochastic approaches, demonstrating that the artificial intelligence models were capable of surpassing the performance of these traditional methods. Feigl et al. (2021) [22] evaluated six artificial intelligence models in highly heterogeneous catchments in Austria and compared these results to air2stream and linear regression. The study demonstrated that machine learning approaches were capable of improving results by up to 64% compared with statistical modelling. Zhu and Pitrowski (2020) [23] review various machine learning techniques and provide a comprehensive overview of artificial intelligence in water temperature modelling. Statistical approaches, irrespective of their nature, possess the significant advantage of predicting water temperature utilizing minimal parameters and with exceptionally brief computation times. Nevertheless, fluctuating conditions can present a substantial challenge for statistical models and artificial intelligence models alike. These methodologies utilize long-term measurement data, and the models are trained on these datasets to elucidate the relationships between the parameters. In the event of a fundamental change, such as the cessation of water extraction at varying temperatures, the temperature regime of the water body undergoes a complete transformation. Given that statistical analyses and most artificial intelligence models are predicated on correlations between one or two parameters, alterations based on parameters not incorporated in these models are not adequately represented. Consequently, such models are not suitable for modelling water temperature in the context of low-flow risk management, as potential mitigation measures cannot be sufficiently represented within the existing frameworks.

Deterministic (process-based) models are predicated on physical processes, which, on the one hand, facilitates highly accurate results, while, on the other hand, necessitating substantial data requirements and computational resources. Considering these aspects, it is imperative to establish an optimal balance between accuracy and practical applica-

bility. Various models are currently extant; however, they possess distinct characteristics, primarily attributable to the specific application objectives of each model. To obtain a comprehensive overview of the diverse models and their availability, we recommend Dugdale et al. (2017) [24]. Information regarding the relevant heat fluxes can also be found in e.g., Webb et al. (2008) [25]. A concise overview of applicable models is presented below.

Westhoff et al. (2007, 2011) [26] present an energy balance model that computes the temperature distribution along a stream by incorporating various energy fluxes, including solar radiation and lateral inflows from groundwater. It utilizes high-resolution temperature data obtained from a sensing system, allowing for precise calibration and a detailed understanding of stream temperature dynamics. The model is well suited; however, the high accuracy requirements of the data may potentially impact its practicability. Gallice et al. (2016) [27] developed the model *StreamFlow*, a semi-distributed model that integrates the simulation of both streamflow discharge and stream temperature, specifically designed for high alpine environments. It employs a modular structure that facilitates various modelling approaches, enhancing the accuracy and reliability of hydrological and thermal predictions in response to climate change. *StreamFlow* is only partially suitable, as the focus on alpine rivers allows only a limited transferability to other rivers. Nevertheless, certain components of the model can be applied to other contexts. The *heatsource* model developed by Boyd and Kasper (2003) [28] is one of the most frequently cited models in the field of water temperature modelling. The model incorporates various heat exchange processes and utilizes highly detailed equations to determine heat fluxes. Factors such as shading due to topography and vegetation, as well as inflowing water, are also taken into consideration. It is therefore frequently utilized as the foundation for more advanced temperature models. The comprehensive consideration of all aspects and the resulting formulae, which necessitate an extensive amount of input data, render the model challenging to implement in certain contexts.

The presented temperature models are individually suitable for modelling river water temperatures. In the context of low-flow risk, the correct representation of influences due to low flow and the transferability to rivers of all sizes and characteristics are of crucial importance. An additional factor influencing model selection is practicability, which is determined by the available input data characteristics in terms of quantity and quality. On the one hand, adequate precision is requisite, as the results are subsequently to be utilized to evaluate the implications of low-flow events. On the other hand, the modelling of long-term time series (e.g., several hundred years) renders computational time a significant factor, which in turn is influenced by the complexity of the model and the volume of data. To fulfil these requirements, components of the aforementioned models are adapted and integrated into a novel water temperature model for a low-flow risk analysis.

2. Materials and Methods

2.1. Framework for Low-Flow Risk Analysis

The modelling of water temperatures in the context of low-flow risk management entails specific requirements. The basis of low-flow risk management is the low-flow risk analysis. Therefore, Satzinger and Bachmann (2024) [10] developed a comprehensive low-flow risk approach to determine the low-flow risk for rivers. The approach encompasses various analyses, which are conducted through methods such as modelling. The fundamental concept involves utilizing long-term time series rather than scenarios, thereby circumventing the complex process of scenario definition. The initial phase of the holistic low-flow risk analysis involves meteorological analysis, employing a statistical weather generator to produce synthetic long-term weather data series. To this end, long-term meteorological data from the meteorological analysis is transformed into discharge time

series in the hydrological analysis. These discharge time series are subsequently utilized as input data for the hydrodynamic analysis, which calculates the water levels, flow velocities and water temperatures in the river. A one-dimensional river model, a bidirectionally coupled two-dimensional groundwater model for the consideration of exfiltration and infiltration, and a unidirectionally coupled one-dimensional water temperature model are employed in this analysis. While bidirectional coupling involves an exchange between the coupled models and consequently mutual influence, unidirectional coupling entails only a transfer of results from the 1D river model to the temperature model, where these are utilized for calculations. Thus, there is no influence of the temperature modelling on the 1D river model, although there is an influence in the opposite way. Based on the outcomes of the hydrodynamic analysis, the assessment of consequences is applied to ascertain the socio-economic and ecological consequences. Subsequently, the losses are aggregated in the risk analysis and divided by the number of modelled years to derive the risk. The requisites from the risk approach to temperature modelling are elucidated in further detail below. The water temperatures must be modelled as a long-term series, analogous to the risk approach. Satzinger and Bachmann (2024) [10] previously noted in their study that calculation time is a crucial factor for practicability. Consequently, the development of a temperature model should consider the computational time required. Another critical aspect is the holistic approach, which necessitates the consideration of a range of factors, including anthropogenic influences. It is imperative that these influences be accurately represented in a temperature model for the purposes of low-flow risk analysis. Furthermore, the transferability between rivers is of significant importance, as the model should be representative of a diverse range of rivers, from small watercourses such as the Selke to large waterways such as the Elbe. The coupling between the one-dimensional river model and the temperature model is unidirectional. Consequently, the results of the river model, specifically the parameters of discharge, flow velocity, water level and width, can be utilized.

2.2. Approach for Water Temperature Modelling

The basis for calculating temperature transport is the one-dimensional heat energy transfer equation, which comprises an advective component and a dispersive component. In the model, the dispersive component is disregarded due to the assumption of complete mixing. Advection describes the transport of temperature along the longitudinal course and is primarily dependent on the flow velocity. In this paper, a specified version of the basic one-dimensional heat advection-dispersion equation by [24,29] is utilized. The basic one-dimensional heat energy transfer equation is as follows:

$$\frac{\delta T}{\delta t} = -U \times \frac{\delta T}{\delta x} + D_L \times \frac{\delta^2 T}{\delta x^2} + \Delta T, \quad (1)$$

where T is the river temperature [K], t is time [s], x is distance [m], U is the average longitudinal flow velocity [m s^{-1}], D_L is the longitudinal dispersion coefficient [$\text{m}^2 \text{s}^{-1}$] and ΔT is the temperature change due to heat fluxes [K s^{-1}]. The advective component of the Equation (1) encompasses the product of flow velocity, as this is crucial for the transport process, while the dispersive component comprises the product of the dispersion coefficient. Equation (1) was reformulated utilizing an implicit upwind scheme due to its inherent stability and robustness in solving advection-dominated transport problems. Unlike explicit schemes, which are often limited by stringent time step constraints to satisfy the Courant–Friedrichs–Lewy (CFL) condition, the implicit approach allows for larger time steps without compromising numerical stability. In the numerical formulation, the cross-sections of the 1D river model represent the spatially discrete nodes, where temperature

and flow properties are computed. The upwind discretization specifically accounts for the direction of flow, ensuring that the solution respects the physical characteristics of advection. This makes it particularly suitable for problems where sharp gradients or steep fronts need to be captured accurately while minimizing numerical diffusion and oscillations [30]. The transformed equation—neglecting dispersion due to assumed complete mixing—is subsequently presented in the following form:

$$\frac{T_i^{j+1} - T_i^j}{\Delta t_i^{j+0.5}} = \frac{-(u_{i-1}^{j+0.5} + u_i^{j+0.5}) \times (T_i^{j+1} - T_{i-1}^{j+1})}{\Delta x} + \Delta t_i^{j+0.5} + \Delta T_i, \quad (2)$$

where T is the river temperature [K], t is time [s], x is distance [m], u is flow velocity [m s^{-1}] and ΔT is the temperature change due to external heat fluxes [K s^{-1}]. The flow velocity can be ascertained from the previous hydraulic computation, given that the interaction between the 1D river model and the temperature model exhibits unidirectional coupling. Inflows are not considered in the formula and must be accounted for separately, which is achieved using Equation (3). As described, the equation considers temperature transport through advection processes and the temperature change due to external heat fluxes. As an upper boundary condition, a hydrograph of water temperature must be specified in the model, ensuring that the first cross-section is always covered by the boundary condition. In the subsequent cross-sections, the temperature calculation is performed using the described method. At the final cross-section, specifying a boundary condition is unnecessary, as the upwind scheme prevents the influence of downstream cross-sections.

The temperature variation in the river is predominantly attributable to exchange processes. Figure 1 presents an overview of the diverse heat fluxes and processes involved in heat exchange and transport, which are denoted by arrows. In addition to the inflows to the river, the heat fluxes φ_{total} calculated in Equation (5) play a crucial role in this phenomenon.

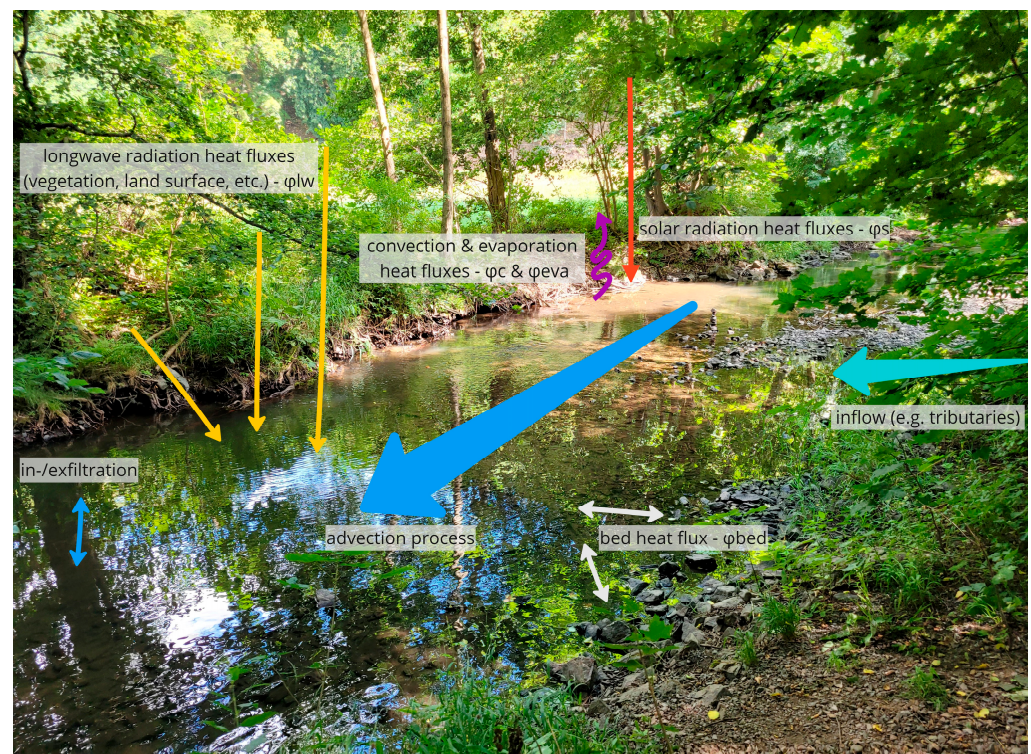


Figure 1. Overview of considered processes in the temperature model (adapted from [23]).

As previously mentioned, the inflow of tributaries or anthropogenic discharge is not considered in Equation (2). To account for inflows from various sources, such as tributaries, groundwater or anthropogenic discharge, the mixing equation from [24,29] is utilized. For this purpose, it is necessary in each calculation timestep to compute the water temperature after complete mixing with the inflowing water instead of calculating the temperature change due to heat fluxes. The selected methodology is deemed appropriate as it offers a straightforward and precise solution for the amalgamation of inflowing water temperatures based on known flow rates and temperatures. This explicit solution is favored as it directly calculates the mixed temperature without necessitating iterative solvers or additional computational complexity. Given that the formula is linear and independent of temporal or spatial discretization, it circumvents potential numerical instability issues, rendering it both efficient and reliable for pre-calculating the initial temperature distribution. This is accomplished using the following formula:

$$T_i^{j+1} = \frac{(T_{i-1}^j \times Q_{i,r}^{j+0.5}) + (T_{i,in}^{j+0.5} \times Q_{i,in}^{j+0.5})}{(Q_{i,r}^{j+0.5} + Q_{i,in}^{j+0.5})}, \quad (3)$$

where Q_r [$\text{m}^3 \text{s}^{-1}$] denotes the discharge of the river itself and Q_{in} [$\text{m}^3 \text{s}^{-1}$] represents the inlet discharge. T_i [K] indicates the temperature prevailing in the river and T_{in} [K] signifies the temperature of the inflowing water.

For the subsequent parameters, as described above, indexing occurs at timestep $j + 0.5$ at location i . For the sake of clarity, this will not be mentioned hereafter.

Temperature changes resulting from radiative influences or exchange processes with the riverbed are accounted for by the term ΔT , which is calculated using the following formula according to [28]:

$$\Delta T = \frac{\varphi_{total}}{\rho_w \times c_w \times wsp}, \quad (4)$$

Herein, φ_{total} [$\text{J m}^{-2} \text{s}^{-1}$] encompasses the sum of all heat fluxes, ρ_w [kg m^{-3}] denotes the density of water, c_w [$\text{J kg}^{-1} \text{K}^{-1}$] represents the specific heat capacity, and wsp [m] signifies the water depth.

The sum of all heat fluxes yields the parameter φ_{total} . The formula was derived from [27].

$$\varphi_{total} = \varphi_{bed} + \varphi_c + \varphi_{eva} + \varphi_{lw} + \varphi_s, \quad (5)$$

The following partial flows are considered: φ_{bed} [$\text{J m}^{-2} \text{s}^{-1}$]—heat flux at the riverbed, φ_c [$\text{J m}^{-2} \text{s}^{-1}$]—heat fluxes from convection, φ_{eva} [$\text{J m}^{-2} \text{s}^{-1}$]—heat fluxes from evaporation, φ_{lw} [$\text{J m}^{-2} \text{s}^{-1}$]—heat fluxes from longwave radiation and φ_s [$\text{J m}^{-2} \text{s}^{-1}$]—heat fluxes from solar radiation. A comprehensive explanation of the calculation of the respective partial flows is provided in Appendix A, as including it here would exceed the scope of this section.

The presented equations constitute the foundational structure of the HYD-Temp temperature model. The HYD-Temp sub model is part of the software package LoFloDes (version 0.1) [31], which is an open-source software written in C++. The model was developed to ascertain the temperature transport and evolution in the longitudinal course of the river. Given that a one-dimensional calculation approach is employed, complete mixing of the river is presumed.

2.3. Case Study

2.3.1. Study Area

As it is intended for holistic low-flow risk analysis, the model necessitates performance across diverse river systems. Consequently, it is evaluated on the Selke, which exemplifies

small creeks, and the Elbe, which is representative of large rivers. The selected rivers are utilized as representative samples to evaluate the effectiveness of the proposed approach. The findings suggest that the approach's effectiveness can be extrapolated to other rivers of similar size. The objective of the proposed approach is not to facilitate a direct transfer of the results to another, albeit similar, catchment. Figure 2 illustrates the geographical locations of the Selke (left) and Elbe (right) rivers in Europe, as well as the land use patterns and topographical elevations within their respective catchments.

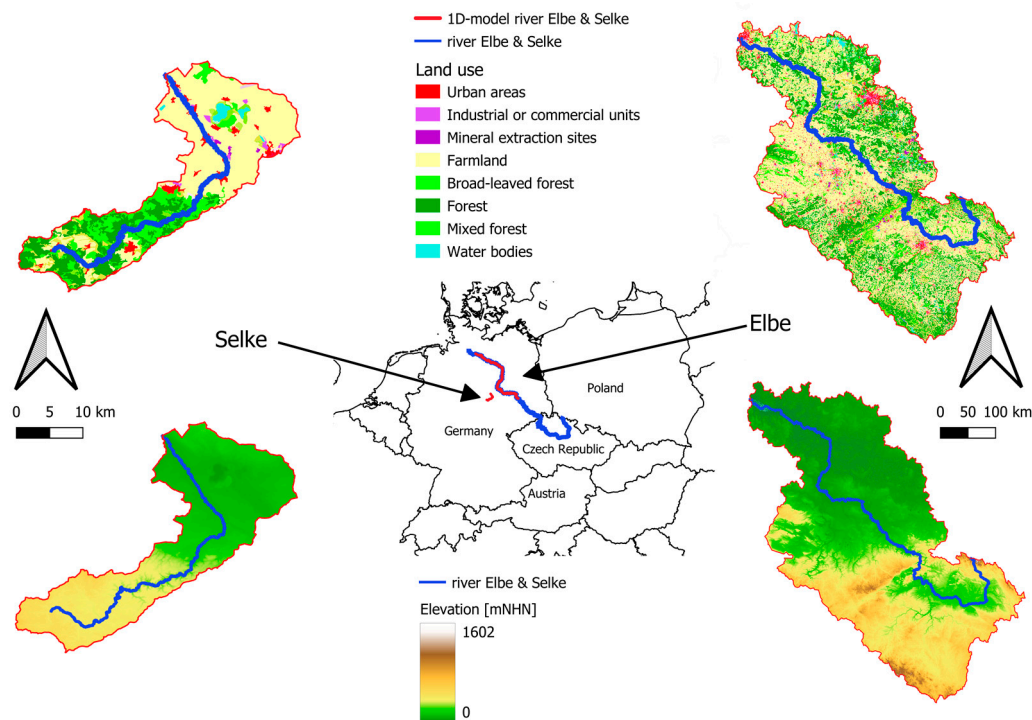


Figure 2. Overview of land use (upper left and right), geographical position (central) and elevation (lower left and right) of the Selke and Elbe rivers.

The Selke (see Figure 2, left), a tributary of the Bode, is part of the Elbe basin in Germany. Spanning 64 km, the Selke drains about 470 km² in the southeastern Harz Mountains. The upper and initial midstream sections of the Selke catchment feature steep terrain with elevations from 150 to 589 m NHN (German height system referencing the Amsterdam Ordnance Datum) and is mainly forested. As the river progresses through lower midstream and downstream areas, it traverses an agricultural lowland with heights between 83 and 150 m NHN. The diverse landscape results in varying precipitation and temperature. The Selke basin has a temperate climate, with average annual rainfall of 660 mm and a mean yearly temperature of about 10 °C. The catchment area has four gauging stations. The Guentersberge gauge, at the Muehlenteich reservoir's outlet in Guentersberge village, monitors a 26 km² catchment area. Water temperature data are available from June 2022 and are influenced by the reservoir. In the upstream part of the Selke, the Silberhuetten gauge oversees a 105 km² catchment, with temperature data available from 1995 onwards. The Meisdorf station, positioned midstream at river km 29.4, covers a 189 km² upstream catchment, marking the end of the mountainous area and the beginning of the lowlands. Water temperatures have been measured since August 1997. Near the river's mouth at river-km 5.5, the Hausneindorf station encompasses almost the entire river catchment, measuring 456 km², with water temperature data available from 2021.

The Middle Elbe is a 490 km long section of the Elbe (see Figure 2, right), which has a total length of 1094 km. It stretches from Castle Hirschstein at river-km 96 to the Geesthacht weir at river-km 586, the last point uninfluenced by the tide. This paper focuses on the part

between Prettin, near the border of Saxony and Saxony-Anhalt, and the Geesthacht weir. Several significant tributaries converge into this section. This segment has been optimized for navigation through groynes. Apart from the Geesthacht weir, the Elbe remains free flowing here. The catchment area is predominantly characterized by agricultural and forestry utilization, and some urban areas. At the Magdeburg-Strombruecke gauge, the average discharge is $544 \text{ m}^3/\text{s}$, and the average low-flow discharge is about $211 \text{ m}^3/\text{s}$. The annual mean air temperature is approximately $10 \text{ }^\circ\text{C}$, placing the region in the temperate climate zone. Various gauges along the river record discharge, water level, and sometimes water temperature. The Elbe catchment area, approximately $148,268 \text{ km}^2$, exhibits highly variable precipitation, ranging from less than 400 mm/a in parts of Saxony-Anhalt to over 1400 mm/a in the Giant Mountains (Czech Republic). The mean annual precipitation is approximately 628 mm . The Elbe originates near the Sněžka at about 1602 mNHN and drains some middle-sized mountain regions. However, less than two percent of the catchment area exceeds 800 mNHN . This is critical for low-flow discharge, as it results in a lack of glacial support and minimal snow contribution, unlike alpine rivers [32]. Low-flow characteristics are influenced by reservoirs, primarily along tributaries, which elevate low water levels. The Elbe has historically experienced many low-flow events, as evidenced by hunger stones [33]. While reservoirs have ameliorated low-flow conditions, several events occurred between 2015 and 2022, with 2018 being particularly notable. The frequency of days with water temperatures exceeding $25 \text{ }^\circ\text{C}$ is increasing [34], and climate change is expected to exacerbate this phenomenon.

2.3.2. Model Set-Up

Usually, long-term data series are utilized for low-flow risk analysis based on Satzinger and Bachmann (2024) [10]. Therefore, long-term meteorological data would be utilized and transformed into runoff series. In this study, however, the temperature model is to be examined as a part of the risk approach. To assess the developed model, it is essential to conduct the evaluation using historical data. Consequently, the period from 1990 to 2020 is modelled on both rivers in order to evaluate the accuracy and applicability of the developed model. During the period under examination, alterations occurred due to changes in land use and construction activities, like removing some weirs along the Selke and a reduction in water abstraction on the Elbe. However, the impact on water temperature remains relatively minor and can therefore be considered negligible. For the Elbe, a one-dimensional river model comprising 4136 cross-sections with an average distance of approximately 100 m was employed. The discharge data of the Elbe itself and the Schwarze Elster, Mulde, Saale, Ohre and Havel tributaries were provided by the Federal Institute of Hydrology (BfG) and applied as boundary conditions. Since 1998, water temperature measurements have been recorded for the Schwarze Elster, Mulde, Saale, and Havel rivers—the most hydrologically significant tributaries of the Middle Elbe—as well as for the Elbe itself at the Dommitzsch gauge station. However, due to data gaps, especially during periods of low flow, statistical modelling was employed using the air2stream model [19] to address these limitations. This enables the generation of complete data series between 1990 and 2020, which are then utilized as boundary conditions in the modelling process. The temperature model's boundary conditions are established using meteorological information obtained from several German Weather Service (DWD) stations. These include Wittenberg, Magdeburg, Seehausen, Boizenburg and Gardelegen (see Figure 3). The requisite meteorological data are obtained from these locations to fulfil the model's requirements. Figure 3 provides an overview of the weather stations (orange) and gauge stations (blue) along the Selke (left) and the Elbe (right).

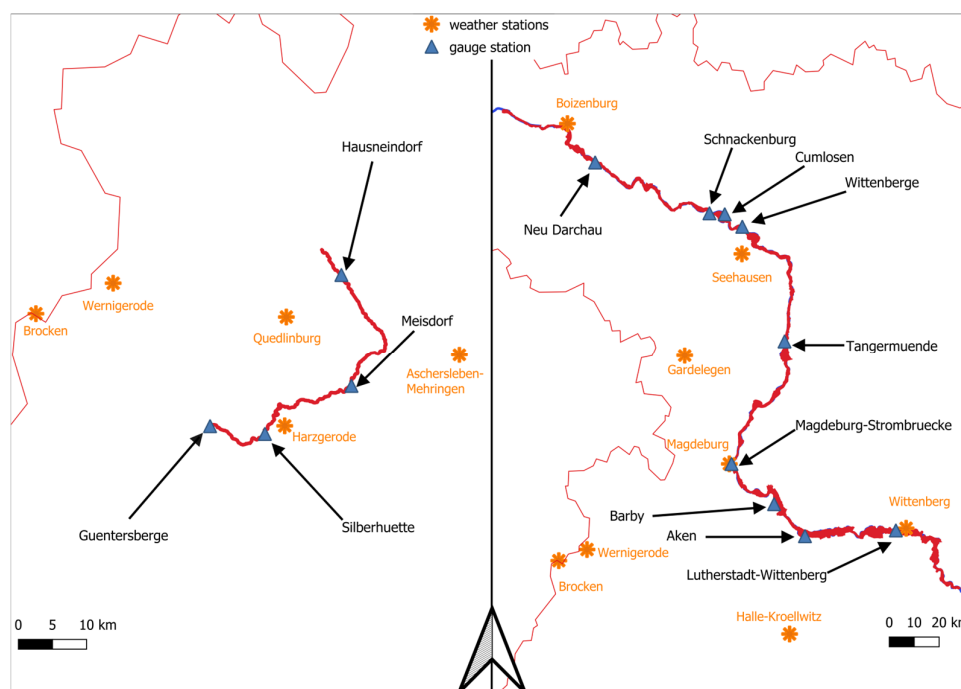


Figure 3. Overview of the different gauge and weather stations along the Selke and Elbe rivers.

A 1D river model was constructed for the Selke with 1247 cross sections and 50 m spacing, extending from Guentersberge gauge to the mouth of the Bode. Discharge data and temperature measurements from Selke gauging stations were provided by the Saxony-Anhalt State Office for Flood Protection and Water Management (LHW). A discharge ratio is determined using measured discharges from tributaries. The discharge at each monitoring point is allocated to two upstream tributaries by the ratio. The remaining discharge is incorporated through diffuse inputs. The groundwater model for near-surface groundwater is under development and not utilized. Due to insufficient data for the temperature model's upper boundary condition, as Guentersberge measurements only started in 2022, we used the *air2stream* [19] to model a time series from 1990 to 2020. Tributary water temperatures were incorporated using measured values, interpolated and applied to other years. The temperature model's boundary conditions use meteorological data from the following German Weather Service (DWD) stations: Harzgerode, Brocken, Halle-Kröllwitz, Wernigerode, Aschersleben-Mehringen, and Quedlinburg.

To determine if the model represents anthropogenic use and altered circumstances accurately, a subsequent simulation is conducted for the rivers. In the second simulation, shading along the Selke was reduced, setting the shading factor uniformly to 50%. This examines whether the model can represent reduced shading effects, such as from regional forest dieback. In the Elbe's second simulation, a heat discharge from a hypothetical industrial plant in Magdeburg was simulated to assess the model's reflection of anthropogenic influences. The model simulates a water withdrawal of $20 \text{ m}^3/\text{s}$, discharged in the Elbe 2000 m downstream with a 4 K temperature increase.

3. Results

3.1. Results for the Selke

Figure 4 compares the results from the 1D river model with the measured values for discharge and water level at the three gauging stations along the Selke. The outcomes of the 1D river model demonstrate a strong correspondence with the annual patterns of the measured discharge curves. Subsequently, statistical metrics are presented to assess the quality of the model results. Some deviations can be seen, mostly during flood periods. For the

low-flow periods the results are quite good. The 1D river model's outcomes, encompassing discharges and water levels, exhibit strong correlation with observed data during low-flow periods across the three Selke gauges. Quality coefficients further validate the model's performance. For river discharge, the Nash–Sutcliffe model efficiency coefficient (NSE, optimal value of 1) [35] yields 0.99 (Silberhuetten), 0.99 (Meisdorf), and 0.97 (Hausneindorf), while the root mean square error (RMSE) amounts to $0.17 \text{ m}^3/\text{s}$ (Silberhuetten), $0.17 \text{ m}^3/\text{s}$ (Meisdorf), and $0.43 \text{ m}^3/\text{s}$ (Hausneindorf), indicating robust model quality. An analysis of water levels below the mean minimum water level reveals RMSE values ranging from 0.07 m at both Silberhuetten and Meisdorf gauges to 0.09 m at the Hausneindorf gauge. Although simulated water levels mirror the pattern of measured data, they frequently surpass or fall short of actual readings. This discrepancy becomes more pronounced during medium and high discharge events. However, the model demonstrates good agreement with measured values during low-flow periods.

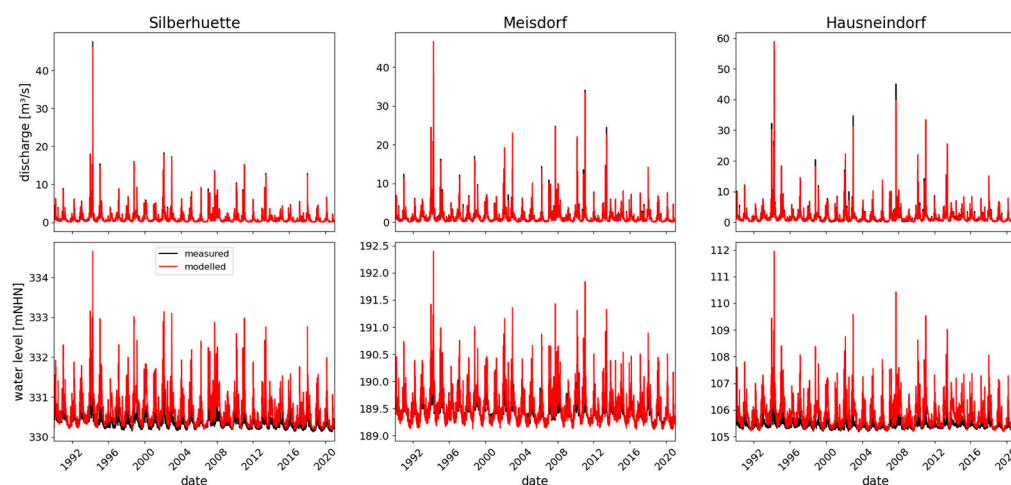


Figure 4. Comparison of modelled and measured discharges and water levels along the Selke.

Figure 5 presents a comparison between the results of the temperature model (red) and measured water temperatures (black) at three gauge stations along the Selke. The measured values are only partially available for Silberhuetten and Meisdorf, as measurements at Hausneindorf commenced in 2021. The upper row displays the complete time series, while the bottom row illustrates a ten-day period between 1 September 2015 and 10 September 2015. This time period represents a low-flow event and serves to demonstrate the correlation with measured values. The low-flow event of 2018 would be well suited for this purpose; however, due to the limited availability of measured values during the low-flow event of 2018, the period of 2015 was selected for analysis. For the temperature model the long-term results show a good alignment with the measured values. It is evident that the model overestimates the water temperature during winter periods. At the Meisdorf gauge, peak temperatures are partially overestimated in the summer months (normally under 2 K), while the highest level of agreement is observed in spring and autumn. Conversely, at the Silberhuetten gauge, the peak temperature in the summer months is underestimated. The observed daily fluctuation range (up to 10 K per day) in the measured values exceeds that of the modelled values (up to 5 K per day). A plausible explanation for this discrepancy is the significant anthropogenic influence, exemplified by the mine water purification plant on the Uhlenbach river. This facility discharges water at a temperature range of 281 to 283 K throughout the year. Analysis of the Silberhuetten gauge yielded an NSE of 0.88 and an RMSE of 1.61 K. Similarly, the Meisdorf gauge exhibited an NSE of 0.85, corresponding to an RMSE of 1.96 K.

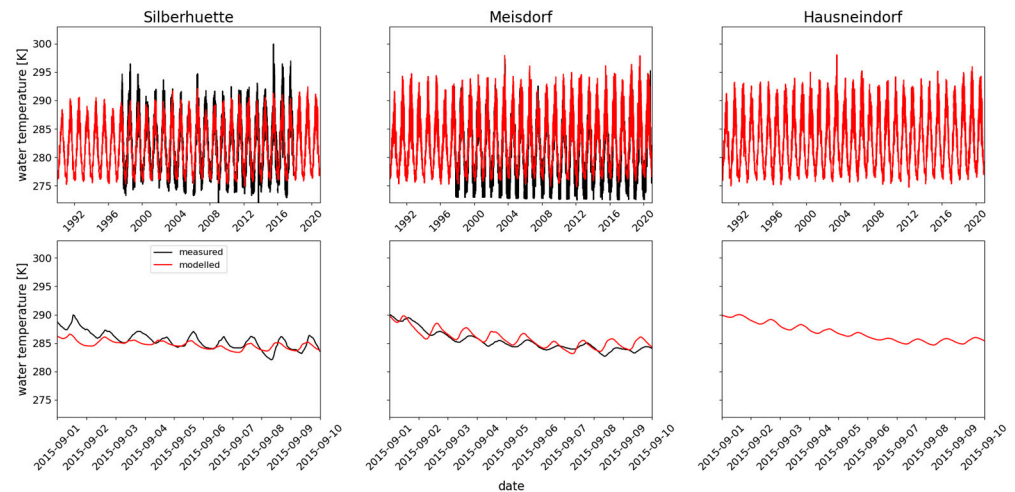


Figure 5. Comparison of modelled and measured water temperature along the Selke (upper part: long-term; bottom part: low-flow period).

Figure 6 shows a longitudinal profile of the temperature gradient along the Selke for three different scenarios (dates) showing the initial condition and the condition with less shading. The water temperature varies along the river and is influenced by the tributaries which are shown as blue vertical lines (dashed blue). The three selected dates represent distinct scenarios: low-flow, summer, and winter. It can be observed that the highest temperatures occur during the summer period and do not necessarily coincide with a low-flow event. The temperature increases along the longitudinal profile of the Selke, which is typical for creeks and small rivers. In winter, the effect of warming along the river course is not evident, as temperatures remain relatively constant. The intra-annual fluctuation range between summer and winter is approximately 15 K. The date 10 September 2018 is representative of low-flow periods, as low-flow conditions prevailed at that time, and the lowest discharges typically occur in this period. It is evident that the water temperature of the Selke during low-flow conditions is significantly influenced by the water temperature of its tributaries. The confluence of the Roedelbach and Uhlenbach rivers results in a decrease in water temperature, which can be attributed to anthropogenic influences (mine water purification plant, Kiliansteich reservoir) on one hand and the naturally cool summer temperatures of those creeks themselves on the other. To obtain an overview of a typical summer day, 29 June 2018 was selected, as the peak temperatures for the entire year occur during the period of June, July and August. The temperature profile is comparable to that observed during low-flow conditions; however, the cooling effect of the tributaries is diminished, and the overall temperatures are elevated. The data from 15 January 2018 represent the temperature gradient during winter periods. It can be clearly observed that temperatures along the river are nearly constant, due to low air temperatures and solar radiation and that there are thus minor changes in temperature due to heat fluxes. The Uhlenbach slightly alters the temperature, due to higher winter temperatures resulting from anthropogenic influence. The longitudinal profiles of the Selke demonstrate that the model adequately reflects the influence of tributaries. The results of the calculation for the condition with less shading demonstrate increased temperatures compared with the initial condition for the summer and low-flow scenarios, which increase along the longitudinal profile. In winter, hardly any difference is discernible. The course of the temperature gradient along the longitudinal profile, however, remains predominantly similar to the initial condition. Nevertheless, it is observable that, particularly in the area of the confluence of tributaries, there is an overlapping effect and a reduced influence of shading.

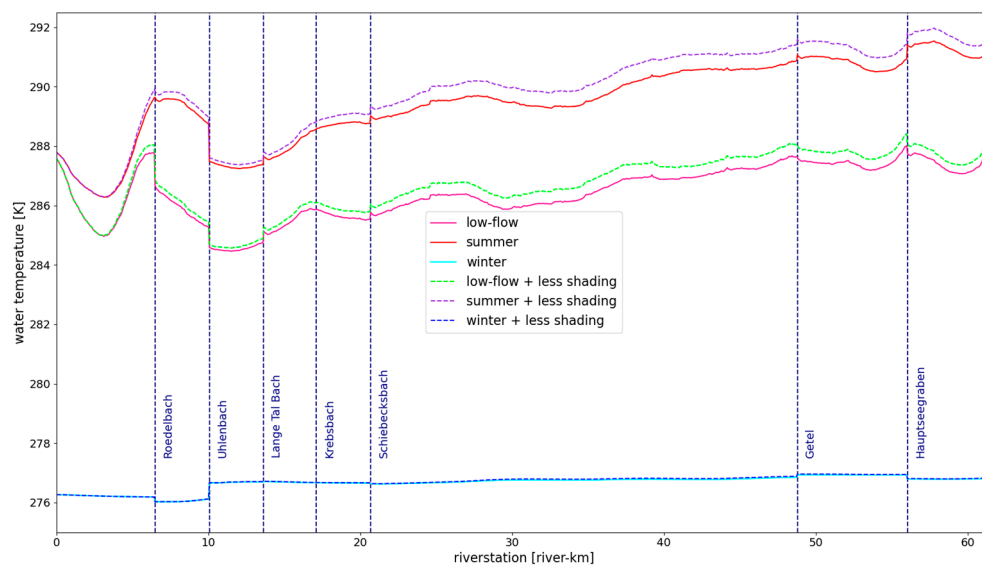


Figure 6. Longitudinal temperature gradient along the Selke River for different scenarios.

The effects of enhanced shading in the upstream and downstream sections of the Selke are illustrated in Figure 7. Figure 7 presents the difference (deep blue) between the modelled results for the initial conditions (red) and the scenario with less shading (green). The bottom row of the plot depicts the difference (blue-grey) between the two conditions. It is evident that warming occurs across all sections. While the maximum deviation at the Silberhuetten gauge remains approximately 0.41 K, the temperature in the Meisdorf area increases by up to 1.08 K compared with the initial condition. At the Hausneindorf gauge, however, the maximum temperature difference is approximately 0.85 K. The minimal increase at the Silberhuetten gauge can be attributed to two factors. Firstly, the upstream section is relatively short, which results in the effect of reduced shading being less pronounced. The influence of the two tributaries, Roedelbach and Uhlenbach, which flow into the Selke shortly before the gauge station, is more significant in determining the temperature development in this section of the Selke (see Figure 6). The cooling effect of these two tributaries is predominant compared with other factors, consequently diminishing the impact of increased radiation due to the less dense shading. The highest warming is observed in the Meisdorf area, which can be explained by the lack of (cooling) tributaries. In contrast, a lower maximum warming was observed at the Hausneindorf gauge, which has the longest upstream flow section compared with the Meisdorf gauge. This can also be explained by the effect of a tributary, namely the Hauptseegraben, which supplies cooling water. The Hauptseegraben flows directly upstream of the gauge and has a significant influence on the water temperature. In addition, the outflow is greater than at the Meisdorf gauge, which is why heating the water requires a higher energy input, which further reduces the influence of reduced shading.

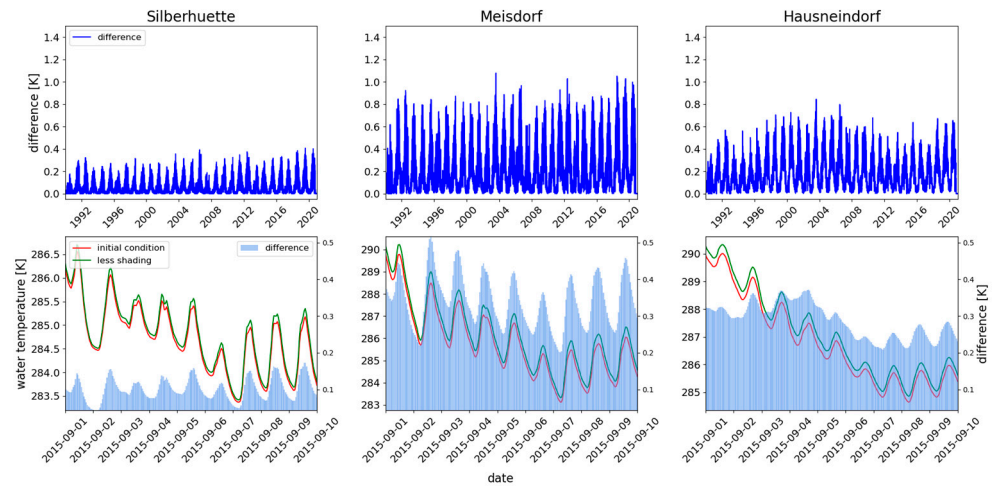


Figure 7. Comparison of the model results for the initial condition and increased shading.

3.2. Results for the Elbe

Figure 8 compares the results from the 1D river model with the measured values at the gauging stations along the Elbe. The results of the hydrodynamic modelling utilizing the 1D river model of the Middle Elbe demonstrate good agreement with the measured discharge curve. Moreover, statistical metrics are employed to illustrate the model’s quality. The NSE value for the modelled discharge at the Lutherstadt-Wittenberg, Aken, Barby, Magdeburg-Strombruecke, Tangermuende and Wittenberge gauge stations is 0.99. Only the Neu Darchau gauge station features an NSE value of 0.98. This indicates a strong correlation between the modelled discharge and the measured discharge. The RMSE, when considering all discharge values, ranges from 41.34 m³/s at Lutherstadt-Wittenberg to 128.82 m³/s at Neu Darchau. During the low-flow periods, the deviations decrease significantly, ranging between 10.06 m³/s at Lutherstadt-Wittenberg and 28.06 m³/s at Neu Darchau. Given the comparatively high discharges, with mean minimum discharges of 138 m³/s at the Lutherstadt-Wittenberg gauge and 275 m³/s at the Neu Darchau gauge, the deviations appear to be tolerable. When solely considering water levels below the mean minimum water level, the RMSE for the calculated water levels ranges from 0.10 m at the Magdeburg-Strombruecke gauge to 0.375 m at the Neu Darchau gauge. Nevertheless, the water levels demonstrate satisfactory concordance, exhibiting minimal deviations at low flow, and can thus serve as a foundation for modelling the water temperature.

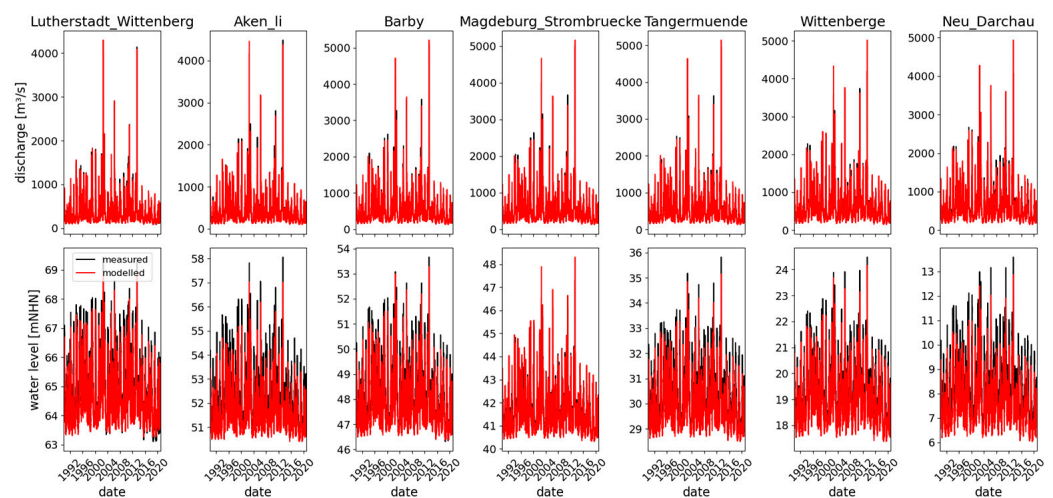


Figure 8. Comparison of modelled and measured discharges and water levels along the Elbe.

Figure 9 compares the results from the water temperature model with the measured temperatures along the Elbe. The modelling of the water temperature demonstrates favorable outcomes along the Elbe. Due to the limited availability of water temperature data, comparison with measured water temperatures is only feasible to a limited extent. At the Lutherstadt-Wittenberg gauge, measurement data are available for the years 2015 to 2017. For this measurement period, the modelled values exhibit an NSE of 0.98 and an RMSE of 0.96 K. The measurement data at the Magdeburg-Strombruecke gauge span from 1995 to 2015, albeit with significant gaps. The concordance of the modelled data, as indicated by the NSE, is 0.97, with an RMSE of 1.14 K. The Cumlosen gauge, which can be seen in Figure 3, has been recording the water temperature of the Elbe since 1997. The NSE is 0.97 and the RMSE is 1.25 K. The most extensive measurement data series is located at the Schnackenburg gauge. The NSE at this location is 0.95 and the RMSE is 1.59 K.

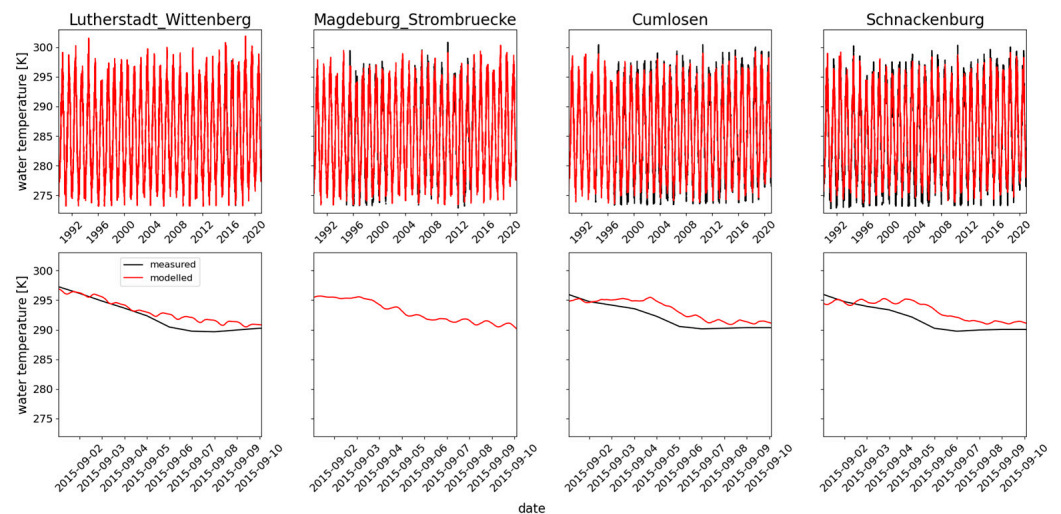


Figure 9. Comparison of modelled and measured water temperature along the Elbe.

Figure 10 illustrates the longitudinal temperature profile of the Elbe for various scenarios. The scenarios are similar to the Selke: summer (29 June 2018), low-flow (10 September 2018) and winter (15 January 2018). The blue dashed vertical lines denote the tributaries considered in temperature modelling, while the dashed orange vertical lines indicate the points where the hypothetical industry park extracts and discharges water back into the Elbe. The water temperature in the longitudinal course of the Elbe exhibits a consistent pattern or slight decrease in both summer and low-flow scenarios. Conversely, during winter, an increase in temperature is observed along the longitudinal course. The highest temperatures are recorded in summer, although the difference compared with low-flow conditions is minimal. The temperature differential between summer and winter is approximately 20 K. The temperature profile indicates that tributaries exert only a marginal influence on the water temperature. This phenomenon is attributable to two factors: firstly, the low water volumes of the tributaries relative to the Elbe discharge, and secondly, the minimal differences in water temperatures. Only the Havel demonstrates a slight influence. The influence of the fictitious industry park is clearly discernible. During the winter months, the influence is minimal and nearly attains the original temperature level shortly after the discharge. In summer, however, there is an observable increase in temperature at the discharge point, which remains elevated until the end of the model, at a distance of over 250 km. The phenomenon is more pronounced during periods of low flow. The rise of the temperature and the deviation from the initial condition are comparable to the trend observed during the summer scenario; however, the increase is more substantial.

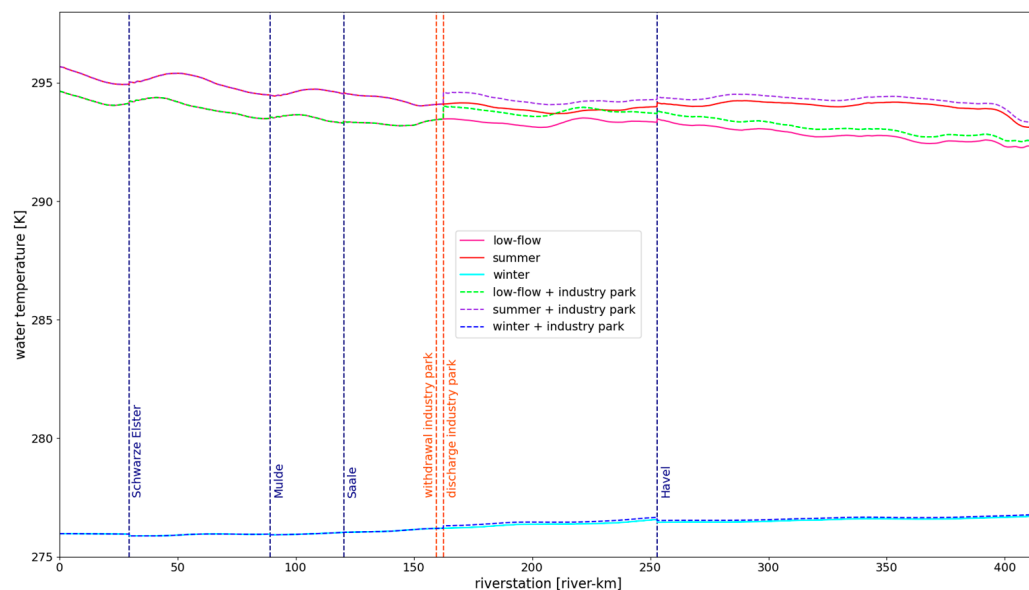


Figure 10. Longitudinal temperature profile along the Elbe.

Figure 11 presents a comparison between the model results for the initial condition (red) and the industrial park (green) with the difference (blue-grey) in the bottom row and the difference over the whole time period in the upper part. To elucidate the influence on a smaller scale, four points are considered: Herrenkrug_bridge (where the water is withdrawn), port_entrance_south (where the heated water is discharged back) and the downstream points port_entrance_north (1000 m) and Autobahn_A2_bridge (5000 m). These points facilitate a more detailed analysis of the small-scale influence, in contrast to Figure 10. At the Herrenkrug bridge, no measurable influence is observed, as the only change is the withdrawal of water from the Elbe. The quantity of water withdrawn alone does not influence the water temperature to a measurable degree. The water from the hypothetical industrial park is discharged about 100 m upstream from the port entrance south site. An increase in water temperature can be observed at this location, with the maximum difference being 0.70 K. It is noteworthy that the greatest deviations occur during low-flow periods, such as those in 2018 and 2019. At the port_entrance_north site, situated approximately 1000 m downstream from the discharge point, an elevation in water temperature remains observable. The maximum deviation from the initial condition is approximately 0.63 K. The Autobahn_A2_bridge site, located approximately 5000 m downstream of the discharge point, also exhibits an increase in water temperature. The maximum deviation of approximately 0.63 K is similar when compared with the upstream observation point. Consequently, the impact of the discharge is detectable over extensive distances and exerts a substantial influence on downstream areas. As Figure 10 points out, there is an influence over the whole river downstream from the discharge point. Nevertheless, it is evident that the temperature differences along the longitudinal profile diminish, and the curves converge further. The influence of thermal pollution on watercourses aligns with the findings of [36].

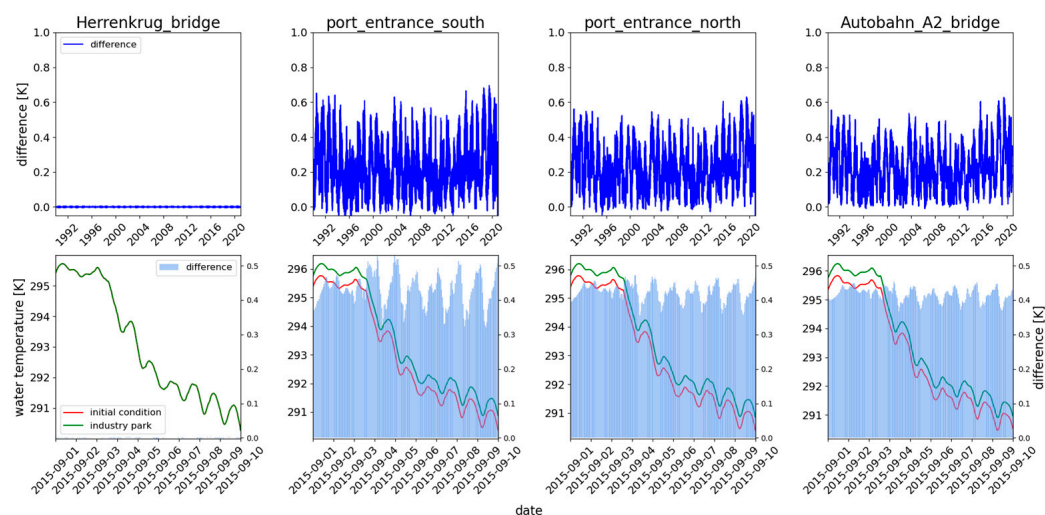


Figure 11. Comparison of the model results for the initial condition and industry park.

4. Discussion

In the context of holistic low-flow risk management, practicability plays a significant role, as it encompasses various aspects that necessitate consideration in the modelling processes. Due to the long-term series of, for example, several hundred years, calculation time can emerge as a substantial disadvantage of the risk approach. The simulations were performed on a Lenovo ThinkPad P15s laptop, equipped with an 11th Gen Intel Core i7-1165G7 processor (4 cores, 2.8 GHz base clock) and 32 GB DDR4 RAM and an NVIDIA Quadro T500 GPU with 4 GB VRAM. The calculation time for the 1D river model in LoFloDes was 220 min for the Selke and 1382 min for the Elbe. The subsequent calculation of the water temperature using HYD-Temp required 110 min for the Selke and 561 min for the Elbe. A period of 31 years was modelled for both rivers, resulting in a calculation time of approximately 10.7 min per modelled year for the Selke and approximately 62.7 min per modelled year for the Elbe. In the context of low-flow risk management with a time series of, for instance, 100 years, the hydrodynamic analysis without a groundwater model results in a calculation time of 1070 min for a small river such as the Selke and 6270 min for a large river such as the Elbe. The computational time enables the execution of multiple model iterations within a feasible timeframe of several weeks. Although these computational requirements necessitate a considerable amount of time, the approach remains suitable for implementation in low-flow risk analysis.

In addition to the aforementioned considerations, the quantity of data required for the calculation is a significant parameter. In the temperature model we presented, the input data requirements are contingent upon the desired output. For instance, if the analysis of consequences necessitates a temporal resolution of 1 h, input data with correspondingly high precision is essential. Conversely, if only weekly values are required as output, data with a lower temporal resolution may suffice. Irrespective of the specific requirements, high-quality data with a high temporal resolution consistently ensure realistic results. The requisite input data for the presented model comprise data from the one-dimensional river model and meteorological data. The necessary meteorological parameters, including air temperature, humidity, global radiation, and wind speed, are available in numerous regions and are frequently accessible to the public. The shading, which must also be taken into consideration, can be estimated utilizing various methodologies, such as those described in Li et al. (2012) [37]. The primary challenge concerning the input data stems from the measured water temperature data of the river and its tributaries. For small and medium-sized rivers, there is often limited or no data available. An additional challenge is presented

by anthropogenic influences from water abstraction or discharges, as there is typically a lack of available data. However, these challenges exist independently of the model. Overall, the effort required to obtain and process data for utilizing the developed model can be classified as moderate. Although alternative models with lower data requirements are available, this is generally at the expense of the accuracy of the results. Conversely, the accuracy of the results can be further enhanced by incorporating additional input parameters, which subsequently increases the data requirements. The model presented here offers an appropriate balance between data requirements and accuracy of the results.

The results of the temperature modelling demonstrate strong correspondence with the measured values for both the Selke and Elbe rivers. The overestimation of water temperature in the winter months, observed in both rivers, is noteworthy. However, given the focus on low-flow periods, which typically occur in summer and autumn, this discrepancy is not of significant concern. The NSE, which quantifies the agreement, and the RMSE, which describes the deviations, are utilized to evaluate the model. The correspondence between the modelled and measured values is highly satisfactory on both rivers, as evidenced by the NSE on the Selke ranging between 0.85 and 0.88, and on the Elbe between 0.95 and 0.98. In the field of hydrological modelling, an NSE between 0.7 and 0.9 is considered good, which indicates the close agreement between modelled and measured values [38]. The mean deviation, as measured by the RMSE, is also low, with values between 0.96 and 1.59 K for the Elbe and 1.61 to 1.96 K for the Selke. In the context of water temperature modelling, RMSEs below 2 are considered indicative of good model performance [39,40]. The developed model demonstrates the capability of simulating diverse rivers ranging from creeks, such as the Selke, to large rivers, such as the Elbe. Consequently, the model fulfils the requirement of low-flow risk management to be applicable to water bodies of diverse types and dimensions. It is also feasible for modeling climate change aspects. Furthermore, the model underwent evaluation to assess its capacity to simulate anthropogenic influences, altered circumstances and potential mitigation measures. The results indicate that the impact of altered circumstances is quantifiable, for both rivers. The influence of anthropogenic discharges was effectively demonstrated through the modelling of a hypothetical industrial park. The model accurately represented the extensive influence that such discharges exert on other water bodies. The findings align with the results of other studies, such as [41,42], although the influence of the discharge depends on numerous factors. It can be concluded that the model effectively depicts altered circumstances and therefore also potential mitigation measures.

The application of a one-dimensional temperature model for large rivers such as the Elbe is subject to debate, as complete mixing does not invariably occur in larger water bodies [43]. It is established that thermal plumes form over distances of several kilometers before mixing occurs. Such phenomena cannot be adequately represented with one-dimensional modelling and necessitate the utilization of a two-dimensional model. This contrasts with the significantly higher computational requirements for a two-dimensional calculation. Despite the detailed results, the relevance in relation to low-flow risk must be critically examined. Two-dimensional modelling appears to be justified only in the context of a detailed analysis of a specific river section, whereas the results of a one-dimensional model are deemed sufficient for a large-scale, long-term analysis as within the low-flow risk analysis.

The results of the model demonstrate the variations in the modelling of different rivers. For instance, shading does not exert a significant influence on the Elbe due to its width, as only a minimal portion of the water surface would be shaded even with dense riparian vegetation. While the tributaries of the Elbe exhibit comparable temperatures, the tributaries of the Selke are crucial for determining the water temperature in the Selke

itself. The Selke is predominantly influenced by the temperatures of its tributaries and the extent of shading, whereas the air temperature exerts the greatest influence on the water temperature in the Elbe. Markovic et al. (2013) [34] put the influence of air temperature on water temperature at 80% in their study. Although the results may not be applicable to all bodies of water, it can be concluded that factors influencing the modelling of small and medium-sized bodies of water differ from those affecting large rivers. This conclusion is also reached by van Vliet et al. (2012) [44].

Further research on water temperature modelling for low-flow conditions should focus on several key areas. First, improving the representation of groundwater–surface water interactions and their impacts on stream temperatures during low-flow periods is needed. This could involve coupling temperature models with more sophisticated groundwater models.

5. Conclusions

The low-flow events of recent years have elucidated the consequences of low-water conditions. It has become evident that the implications of low water are frequently not attributable to complete desiccation of the water body, but rather to an interaction between low discharge rates and a (resulting) deterioration in water quality. A parameter of central importance in this context is water temperature, as it significantly influences both ecological and economic water users. To address the consequences of elevated water temperatures during low-flow conditions, a low-flow risk management strategy can be established. This approach utilizes a holistic methodology, which considers all aspects from origin (weather/hydrology) through expression (hydrodynamic) to consequences. A component of the hydrodynamic analysis is a model for determining water temperature. This study developed and evaluated a water temperature model optimized to integrate into low-flow risk analysis.

The developed model is a one-dimensional water temperature model using unidirectional coupling to the 1D river model. The developed temperature model demonstrates high performance in simulating water temperatures for both small rivers (Selke) and large rivers (Elbe), with NSE values ranging from 0.85 to 0.98 and RMSE values of 0.96 to 1.96 K. The model effectively represents anthropogenic influences, altered circumstances and potential mitigation measures, such as a change in riparian shading or industrial discharges.

Water temperature in rivers is influenced by multiple factors, with river size playing a pivotal role in determining the predominant influences. In smaller rivers, such as the Selke, tributaries and shading exert a more significant impact on water temperature. Conversely, in larger rivers, like the Elbe, air temperature emerges as the primary determinant of water temperature. This knowledge is essential in terms of the desired broad applicability in the context of low-flow risk management. The selection of an appropriate modelling approach is contingent upon the specific requirements of the analysis. A one-dimensional model offers an optimal balance between accuracy and computational efficiency, rendering it suitable for long-term risk assessments. However, for detailed examinations of specific river sections, a two-dimensional modelling approach may be more appropriate. A challenge of low-flow risk management is to obtain enough data, which is often difficult. Therefore, it is noteworthy that water temperature modelling faces challenges related to data availability, particularly concerning water temperatures of tributaries and anthropogenic influences. Notwithstanding these challenges, the model's computational efficiency, requiring 3.5–18 (with 1D river model 10–63) minutes per modelled year, facilitates practical implementation in low-flow risk analysis over extended periods.

The realistic modelling of water temperature is a central aspect of low-flow risk analysis, as it is utilized in various analyses. While temperature modelling is executed

in the hydrodynamic analysis, the results are employed as input data for the analysis of consequences. Considering the consequences of elevated water temperatures for ecology, as well as socio-economic water users, the significance of temperature modelling in risk analysis becomes evident.

In conclusion, the developed temperature model fulfills the requirements for integration into holistic low-flow risk management frameworks. It provides a valuable tool for assessing temperature-related impacts and evaluating mitigation strategies across diverse river systems. Future research should focus on improving the representation of groundwater–surface water interactions and on further validating the model across a wider range of river types and climate conditions.

Author Contributions: Conceptualization, U.S.; methodology, U.S. and D.B.; software, D.B.; validation, U.S.; investigation, U.S.; data curation, U.S.; writing—original draft preparation, U.S.; writing—review and editing, U.S. and D.B.; visualization, U.S.; supervision, D.B.; project administration, D.B.; funding acquisition, D.B. All authors have read and agreed to the published version of the manuscript.

Funding: This research was conducted as part of the DryRivers project, which was funded within the WaX—Water Extreme Events grant from the Federal Ministry of Education and Research (BMBF) (FKZ 02WEE1628A). The APC was funded through DryRivers project funds.

Data Availability Statement: The data used in this study, except for the discharge and measured temperature data of the Elbe, are available upon reasonable request. Similarly, the software (LOFLODES: <https://github.com/dabachma/LoFloDes>, version 0.1, accessed on 15 February 2025) and Python (version 3.10) scripts used are also available.

Acknowledgments: We extend our gratitude to the Landesbetrieb für Hochwasserschutz und Wasserwirtschaft Sachsen-Anhalt and the Federal Institute of Hydrology/Bundesanstalt für Gewässerkunde for furnishing the discharge and water temperature of the river Selke and Elbe. During the preparation of this work the authors used paperpalAI (version 2.17.0)/Cactus Communications in order to improve the language used and help create a consistent paper. After using this tool/service, the authors reviewed and edited the content as needed and take full responsibility for the content of the publication.

Conflicts of Interest: The authors declare no conflicts of interest.

Appendix A

The subsequent section provides a comprehensive explanation of the methodology employed in calculating the heat fluxes.

The heat fluxes at the bed of the watercourse are represented by the parameter φ_{bed} . For the calculation, the approach of [27] was selected.

$$\varphi_{bed} = k_{bed} \times [T_{bed} - T_w], \quad (A1)$$

where T_{bed} [K] represents the temperature of the riverbed, T_w [K] denotes the water temperature, and k_{bed} [$\text{W m}^{-2} \text{K}^{-1}$] characterizes the thermal conductivity of the bed material.

Convection heat flux, which is often referred to as sensible heat flux, describes the energy transfer at the water–air interface resulting from heat exchange due to temperature differentials between the two media. In this context, the temperature gradient is represented by the Bowen ratio, which functions as a proportionality constant between the convection flux and the evaporation flux at the air–water interface. Consequently, this ratio is contingent upon the temperatures of both the stream and the air, as well as the vapor

pressure [45]. The Bowen ratio is represented in the following equation from [28], using the factors excluding φ_{eva} :

$$\varphi_c = \varphi_{eva} \times 0.00061 \times P_a \times \frac{[T_w - T_{air}]}{(e_{s^*} - e_{a^*})}, \quad (A2)$$

$$e_{s^*} = 6.1275 \times e^{\frac{17.27 \times T_{w,c}}{(237.3 + T_{w,c})}}, \quad (A3)$$

$$e_{a^*} = e_{s^*} \times H, \quad (A4)$$

where P_a [mbar] represents atmospheric pressure, T_w [K] denotes water temperature, and T_{air} [K] signifies air temperature. The saturation vapor pressure e_{s^*} [-] and the prevailing vapor pressure e_{a^*} [-] are calculated utilizing $T_{w,c}$ [°C] and humidity H [-].

As water molecules in the liquid phase acquire thermal and kinetic energy, they overcome intermolecular forces and transition to the vapor phase. A low vapor pressure in the atmosphere above the water body facilitates the retention of more water molecules in the gaseous state, while high vapor pressure increases molecular collisions, thereby reducing evaporation. When the air reaches its saturation vapor pressure, evaporation ceases, and condensation may occur, resulting in the transfer of heat back to the water. The latent heat of vaporization plays a pivotal role in this process, and evaporation constitutes the primary mechanism by which streams dissipate heat, thereby influencing water temperature. Precise estimation of evaporation flux is essential for simulating heat dissipation in streams. In the presented model, the equations from [26] were utilized to assess latent heat flux.

$$\varphi_{eva} = -p_w \times L_E \times E, \quad (A5)$$

$$L_E = 1000 \times (2501.4 + T_w) = 1, \quad (A6)$$

$$E = \frac{s \times \varphi_r}{p_w \times L_e \times (s + \gamma)} + \frac{c_{air} \times p_{air} \times (e_s - e_a)}{p_w \times L_e \times r_a (s + \gamma)}, \quad (A7)$$

$$s = \frac{4100 \times e_s}{(237 + T_{air})^2}, \quad (A8)$$

$$r_a = \frac{245}{0.54 \times v_{wind} + 0.5} = 1, \quad (A9)$$

Finally, φ_{eva} is the product of the density of water p_w [kg m⁻³], the latent heat of evaporation L_E and the open water evaporation rate E [ms⁻¹]. Other parameters utilized are aerodynamic resistance r_a [s m⁻¹]; slope of vapor pressure for current temperature s [kPa K⁻¹]; φ_r [W m⁻²], which is the sum of radiation fluxes; specific heat capacity of air c_{air} [J kg⁻¹ K⁻¹]; density of air p_{air} [kg m⁻³]; psychrometric constant γ [kPa K⁻¹]; and wind velocity v_{wind} [m s⁻¹]. The saturation vapor pressure, as well as prevailing vapor pressure, is calculated utilizing Equation (A3) but using T_{air} [K] instead of $T_{w,c}$ [°C].

Longwave radiation contains three different radiations: atmospheric longwave radiation, back radiation (from water surface) and land cover longwave radiation. The following equations are from [26,29]

$$\varphi_{lw} = \varphi_{atw} + \varphi_{lclw} + \varphi_{slw}, \quad (A10)$$

$$\varphi_{atw} = 0.96 \times vts \times \varepsilon_{atm} \times \sigma \times T_{air}^4, \quad (A11)$$

$$\varphi_{lclw} = 0.96 \times (1 - vts) \times \varepsilon_{atm} \times \sigma \times T_{air}^4, \quad (A12)$$

$$\varphi_{slw} = -0.96 \times \sigma \times T_w^4, \quad (A13)$$

$$\varepsilon_{atm} = 1.1 \times B_c + 0.094 \times \sqrt{e_a}, \quad (A14)$$

The longwave radiation heat fluxes are the sum of atmospheric longwave heat flux φ_{atw} [W m^{-2}], landcover longwave heat flux φ_{lclw} [W m^{-2}] and back radiation from the water column φ_{slw} [W m^{-2}]. Consequently, the view-to-sky coefficient vts [-] is requisite, as it quantifies the density of vegetation and facilitates the determination of weights between atmospheric and land cover heat fluxes. The emissivity of the atmosphere ε_{atm} [-] and the Brunt coefficient B_c [-] are shown in (A14).

Solar radiation is categorized into two components: direct solar radiation and diffusive solar radiation. The heat fluxes resulting from solar radiation are calculated using the adapted equation from [26]:

$$\varphi_s = (1 - D_f) \times (\varphi_{direct} + \varphi_{diffusive}), \quad (\text{A15})$$

$$\varphi_{direct} = s_F \times (1 - D_{diffusive}) \times \varphi_{gr}, \quad (\text{A16})$$

$$\varphi_{diffusive} = D_{diffusive} \times \varphi_{gr}, \quad (\text{A17})$$

The solar heat fluxes φ_s [W m^{-2}] are determined by calculating the fraction of radiation that directly heats the water. This is calculated by subtracting the fraction that warms the riverbed D_f [-] from one and multiplying it by the sum of direct φ_{direct} [W m^{-2}] and diffuse $\varphi_{diffusive}$ [W m^{-2}] heat fluxes. To determine the relative contributions of diffuse and direct solar radiation, the factor $D_{diffusive}$ [-] is utilized and applied to the measured global radiation φ_{gr} [W m^{-2}]. For direct solar radiation, the extent of shading must be considered by employing the shadow factor s_F [-].

Table A1 provides an overview of the parameters utilized.

Table A1. Parameters of the water temperature model.

Parameter	Symbol	Unit	Value Range
Density of water	ρ_w	kg m^{-3}	1000
Heat capacity of water	c_w	$\text{J kg}^{-1} \text{K}^{-1}$	4195
Density of air	ρ_{air}	kg m^{-3}	1.2
Heat capacity of air	c_{air}	$\text{J kg}^{-1} \text{K}^{-1}$	1015
Water level	wsp	m	0–25
Heat transfer coefficient	k_{bed}	$\text{W m}^{-2} \text{K}^{-1}$	3–52
Air pressure	P_a	mbar	1013
Humidity	H	-	0–1
Psychrometric constant	γ	kPa K^{-1}	0.67
Wind velocity	v_{wind}	m s^{-1}	0–150
View-to-sky coefficient	vts	-	0–1
Stefan–Boltzmann constant	σ	$\text{W m}^{-2} \text{K}^{-1}$	5.67×10^{-8}
Brunt coefficient	B_c	-	0.6–0.7
Fraction of radiation which reaches the streambed	D_f	%	0–1
Shadow factor	s_F	-	0–1
Fraction of diffusive solar radiation	$D_{diffusive}$	-	0–1
Air temperature	T_{air}	K	250–315
Water temperature	T_w	K	273–310

References

1. Internationale Kommission zum Schutz des Rheins. Bericht zum Niedrigwasserereignis Juli–November 2018 No. 263, Koblenz. 2020. Available online: <https://www.iksr.org/de/oeffentliches/dokumente/archiv/fachberichte/fachberichte-einzeldarstellung/263-bericht-zum-niedrigwasserereignis-juli-november-2018> (accessed on 4 July 2023).
2. Low Water Levels May Further Restrict Output at France’s Chooz Nuclear Plant. *Reuters Media*, 18 August 2020. Available online: <https://www.reuters.com/article/markets/commodities/low-water-levels-may-further-restrict-output-at-france-s-chooz-nuclear-plant-idUSL8N2FK4X7/> (accessed on 2 December 2024).

3. Guénand, Y.; Gailhard, J.; Monteil, C.; Peton, P.-Y.; Martinet, C.; Collet, L.; Bono, C. Climate change impact on nuclear power outages—Part I: A methodology to estimate hydro-thermic environmental constraints on power generation. *Energy* **2024**, *307*, 132648. [CrossRef]
4. GRS gmbH. Half of the Reactor Fleet off the Grid—The Causes of the Standstills in France. Available online: <https://www.grs.de/en/news/half-reactor-fleet-grid-causes-standstills-france> (accessed on 2 December 2024).
5. Cammalleri, C.; Naumann, G.; Mentaschi, L.; Formetta, G.; Forzieri, G.; Gosling, S.; Bisselink, B.; de Roo, A.; Feyen, L. *Global Warming and Drought Impacts in the EU: JRC PESETA IV Project: Task 7*; Publications Office of the European Union: Luxembourg, 2020; ISBN 978-92-76-12947-9.
6. Starck, S.; Wolter, C. Resilience Approach for Assessing Fish Recovery after Compound Climate Change Effects on Algal Blooms. *Sustainability* **2024**, *16*, 5932. [CrossRef]
7. Bayerisches Landesamt für Umwelt. Niedrigwasser 2018 und 2019: Analysen und Auswirkungen für Bayern, Augsburg. 2021. Available online: [https://www.bestellen.bayern.de/application/eshop_app000000?SID=1548206939&DIR=eshop&ACTIONxSETVAL\(artdtl.htm,APGxNODENR:3771,AARTxNR:ifu_was_00198,AARTxNODENR:357889,USERxBODYURL:artdtl.htm,KATALOG:StMUG,AKATxNAME:StMUG,ALLE:x\)=X](https://www.bestellen.bayern.de/application/eshop_app000000?SID=1548206939&DIR=eshop&ACTIONxSETVAL(artdtl.htm,APGxNODENR:3771,AARTxNR:ifu_was_00198,AARTxNODENR:357889,USERxBODYURL:artdtl.htm,KATALOG:StMUG,AKATxNAME:StMUG,ALLE:x)=X) (accessed on 27 June 2023).
8. Hoess, R.; Geist, J. Spatiotemporal variation of streambed quality and fine sediment deposition in five freshwater pearl mussel streams, in relation to extreme drought, strong rain and snow melt. *Limnologica* **2020**, *85*, 125833. [CrossRef]
9. Khan, M.D.; Shakya, S.; Vu, H.H.T.; Ahn, J.W.; Nam, G. Water Environment Policy and Climate Change: A Comparative Study of India and South Korea. *Sustainability* **2019**, *11*, 3284. [CrossRef]
10. Satzinger, U.; Bachmann, D. Conceptual approach for a holistic low-flow risk analysis. *Hydrol. Process.* **2024**, *38*, e15217. [CrossRef]
11. van Vliet, M.T.H.; Ludwig, F.; Zwolsman, J.J.G.; Weedon, G.P.; Kabat, P. Global river temperatures and sensitivity to atmospheric warming and changes in river flow. *Water Resour. Res.* **2011**, *47*, W02544. [CrossRef]
12. Booker, D.J.; Whitehead, A.L. River water temperatures are higher during lower flows after accounting for meteorological variability. *River Res. Apps* **2022**, *38*, 3–22. [CrossRef]
13. Ionita, M.; Nagavciuc, V. Forecasting low flow conditions months in advance through teleconnection patterns, with a special focus on summer 2018. *Sci. Rep.* **2020**, *10*, 13258. [CrossRef]
14. Rothstein, B.; Müller, U.; Greis, S.; Scholten, A.; Schulz, J.; Nilson, E. Elektrizitätsproduktion im Kontext des Klimawandels—Auswirkungen der sich ändernden Wassertemperaturen und des sich verändernden Abflussverhaltens. *Korrespondenz Wasser-wirtschaft.* **2008**, *10*, 555–561. [CrossRef]
15. Durmayaz, A.; Sogut, O.S. Influence of cooling water temperature on the efficiency of a pressurized-water reactor nuclear-power plant. *Int. J. Energy Res.* **2006**, *30*, 799–810. [CrossRef]
16. Arismendi, I.; Safeeq, M.; Johnson, S.L.; Dunham, J.B.; Haggerty, R. Increasing synchrony of high temperature and low flow in western North American streams: Double trouble for coldwater biota? *Hydrobiologia* **2013**, *712*, 61–70. [CrossRef]
17. Bradford, M.J.; Heinonen, J.S. Low Flows, Instream Flow Needs and Fish Ecology in Small Streams. *Can. Water Resour. J.* **2008**, *33*, 165–180. [CrossRef]
18. Rabi, A.; Hadzima-Nyarko, M.; Šperac, M. Modelling river temperature from air temperature: Case of the River Drava (Croatia). *Hydrol. Sci. J.* **2015**, *60*, 1490–1507. [CrossRef]
19. Toffolon, M.; Piccolroaz, S. A hybrid model for river water temperature as a function of air temperature and discharge. *Environ. Res. Lett.* **2015**, *10*, 114011. [CrossRef]
20. Benyahya, L.; Caissie, D.; St-Hilaire, A.; Ouarda, T.B.; Bobée, B. A Review of Statistical Water Temperature Models. *Can. Water Resour. J.* **2007**, *32*, 179–192. [CrossRef]
21. Zhu, S.; Nyarko, E.K.; Hadzima-Nyarko, M. Modelling daily water temperature from air temperature for the Missouri River. *PeerJ* **2018**, *6*, e4894. [CrossRef]
22. Feigl, M.; Lebiezinski, K.; Herrnegger, M.; Schulz, K. Machine-learning methods for stream water temperature prediction. *Hydrol. Earth Syst. Sci.* **2021**, *25*, 2951–2977. [CrossRef]
23. Zhu, S.; Piotrowski, A.P. River/stream water temperature forecasting using artificial intelligence models: A systematic review. *Acta Geophys.* **2020**, *68*, 1433–1442. [CrossRef]
24. Dugdale, S.J.; Hannah, D.M.; Malcolm, I.A. River temperature modelling: A review of process-based approaches and future directions. *Earth-Sci. Rev.* **2017**, *175*, 97–113. [CrossRef]
25. Webb, B.W.; Hannah, D.M.; Moore, R.D.; Brown, L.E.; Nobilis, F. Recent advances in stream and river temperature research. *Hydrol. Process.* **2008**, *22*, 902–918. [CrossRef]
26. Westhoff, M.C.; Savenije, H.H.G.; Luxemburg, W.M.; Stelling, G.S.; van de Giesen, N.C.; Selker, J.S.; Pfister, L.; Uhlenbrook, S. A distributed stream temperature model using high resolution temperature observations. *Hydrol. Earth Syst. Sci.* **2007**, *11*, 1469–1480, Erratum in *Hydrol. Earth Syst. Sci.* **2011**, *15*, 3091. <https://doi.org/10.5194/hess-15-3091-2011>. [CrossRef]

27. Gallice, A.; Bavay, M.; Brauchli, T.; Comola, F.; Lehning, M.; Huwald, H. StreamFlow 1.0: An extension to the spatially distributed snow model Alpine3D for hydrological modeling and deterministic stream temperature prediction. *Geosci. Model Dev. Discuss.* **2016**, *9*, 4491–4519. [[CrossRef](#)]
28. Boyd, M.; Kasper, B. Analytical Methods for Dynamic Open Channel Heat and Mass Transfer: Methodology for the Heat Source Model Version 7.0. 2003. Available online: <https://www.oregon.gov/deq/FilterDocs/heatsourcemanual.pdf> (accessed on 10 January 2025).
29. Sinokrot, B.A.; Stefan, H.G. Stream temperature dynamics: Measurements and modeling. *Water Resour. Res.* **1993**, *29*, 2299–2312. [[CrossRef](#)]
30. Patankar, S.V. *Numerical Heat Transfer and Fluid Flow*; CRC Press: Boca Raton, FL, USA, 1980; ISBN 9781315275130.
31. LoFloDes. Available online: <https://github.com/dabachma/LoFloDes> (accessed on 10 February 2025).
32. International Commission for the Protection of the Elbe River. The Elbe River and Its Basin. Available online: https://www.ikse-mkol.org/fileadmin/media/user_upload/E/06_Publikationen/08_IKSE_Flyer/2016_ICPER-Flyer_The_Elbe_River_Basin.pdf (accessed on 14 January 2025).
33. Elleder, L.; Kašpárek, L.; Šírová, J.; Kabelka, T. Low water stage marks on hunger stones: Verification for the Elbe from 1616 to 2015. *Clim. Past* **2020**, *16*, 1821–1846. [[CrossRef](#)]
34. Markovic, D.; Scharfenberger, U.; Schmutz, S.; Pletterbauer, F.; Wolter, C. Variability and alterations of water temperatures across the Elbe and Danube River Basins. *Clim. Change* **2013**, *119*, 375–389. [[CrossRef](#)]
35. Moriasi, D.N.; Arnold, J.G.; van Liew, M.W.; Bingner, R.L.; Harmel, R.D.; Veith, T.L. Model Evaluation Guidelines for Systematic Quantification of Accuracy in Watershed Simulations. *Trans. ASABE* **2007**, *50*, 885–900. [[CrossRef](#)]
36. Zhang, H.; Kang, M.; Wu, J.; Wang, C.; Li, J.; Du, H.; Yang, H.; Wei, Q. Increasing River Temperature Shifts Impact the Yangtze Ecosystem: Evidence from the Endangered Chinese Sturgeon. *Animals* **2019**, *9*, 583. [[CrossRef](#)]
37. Li, G.; Jackson, C.R.; Kraseski, K.A. Modeled riparian stream shading: Agreement with field measurements and sensitivity to riparian conditions. *J. Hydrol.* **2012**, *428–429*, 142–151. [[CrossRef](#)]
38. Koch, H.; Grünewald, U. Regression models for daily stream temperature simulation: Case studies for the river Elbe, Germany. *Hydrol. Process.* **2010**, *24*, 3826–3836. [[CrossRef](#)]
39. Caissie, D.; Satish, M.G.; El-Jabi, N. Predicting water temperatures using a deterministic model: Application on Miramichi River catchments (New Brunswick, Canada). *J. Hydrol.* **2007**, *336*, 303–315. [[CrossRef](#)]
40. Laanaya, F.; St-Hilaire, A.; Gloaguen, E. Water temperature modelling: Comparison between the generalized additive model, logistic, residuals regression and linear regression models. *Hydrol. Sci. J.* **2017**, *62*, 1078–1093. [[CrossRef](#)]
41. Xu, D.; Wang, H.; Han, D.; Chen, A.; Niu, Y. Phytoplankton community structural reshaping as response to the thermal effect of cooling water discharged from power plant. *Environ. Pollut.* **2021**, *285*, 117517. [[CrossRef](#)] [[PubMed](#)]
42. Sinokrot, B.A.; Gulliver, J.S. In-stream flow impact on river water temperatures. *J. Hydraul. Res.* **2000**, *38*, 339–349. [[CrossRef](#)]
43. Lane, S.N.; Parsons, D.R.; Best, J.L.; Orfeo, O.; Kostaschuk, R.A.; Hardy, R.J. Causes of rapid mixing at a junction of two large rivers: Río Paraná and Río Paraguay, Argentina. *J. Geophys. Res.* **2008**, *113*, F02024. [[CrossRef](#)]
44. van Vliet, M.T.H.; Yearsley, J.R.; Franssen, W.H.P.; Ludwig, F.; Haddeland, I.; Lettenmaier, D.P.; Kabat, P. Coupled daily streamflow and water temperature modelling in large river basins. *Hydrol. Earth Syst. Sci.* **2012**, *16*, 4303–4321. [[CrossRef](#)]
45. Bowen, I.S. The Ratio of Heat Losses by Conduction and by Evaporation from any Water Surface. *Phys. Rev.* **1926**, *27*, 779–787. [[CrossRef](#)]

Disclaimer/Publisher’s Note: The statements, opinions and data contained in all publications are solely those of the individual author(s) and contributor(s) and not of MDPI and/or the editor(s). MDPI and/or the editor(s) disclaim responsibility for any injury to people or property resulting from any ideas, methods, instructions or products referred to in the content.